Journal of
Composites Science

MDPI

Article

Stress Analysis of Tibial Bone Using Three Different Materials for Bone Fixation Plates

Mario Ceddia [1,*], Giuseppe Solarino [2], Maria Tucci [2], Luciano Lamberti [1] and Bartolomeo Trentadue [1]

[1] Department of Mechanics, Mathematics and Management, Polytechnic of Bari, 70125 Bari, Italy; luciano.lamberti@poliba.it (L.L.); bartolomeo.trentadue@poliba.it (B.T.)
[2] Department of Translational Biomedicine and Neuroscience, University of Bari "Aldo Moro", Policlinico, Piazza G. Cesare, 11, 70124 Bari, Italy; giuseppe.solarino@uniba.it (G.S.); tuccim.199@gmail.com (M.T.)
* Correspondence: marioceddia1998@gmail.com

Abstract: Stress shielding is a problem for traditional metal bone fixation plates made of magnesium and titanium alloys. This problem can be solved by using composite materials with a low elastic modulus. This study analyzed the effect of carbon fiber reinforced PEEK (CFRP) composites on stress shielding under static loading using finite element simulations. Callus formation times relative to the healing period were gradually imposed according to the elapsed time, considering 1% and 75% as healing stages. The Inventor© 3D CAD 2024 software was used for modeling, and the ANSYS© FEA R2023 software was used for analysis. The results showed that metal fixation plates made of titanium and magnesium alloys transferred less stress to the bone than the CFRP fixation plate. In particular, the use of the CFRP fixation plate resulted in a higher peak stress and a more uniform stress field in the bone, especially in the bone-plate contact area, where the risk of stress shielding is higher in the 1% and 75% healing phases.

Keywords: human tibia fractures; fixation plates; metallic alloys; CFRP; stress shielding; finite element analysis

Citation: Ceddia, M.; Solarino, G.; Tucci, M.; Lamberti, L.; Trentadue, B. Stress Analysis of Tibial Bone Using Three Different Materials for Bone Fixation Plates. *J. Compos. Sci.* **2024**, *8*, 334. https://doi.org/10.3390/jcs8090334

Academic Editor: Prashanth Konda Gokuldoss

Received: 29 July 2024
Revised: 16 August 2024
Accepted: 22 August 2024
Published: 23 August 2024

1. Introduction

Human tibia fractures are common bone injuries due to falls or traffic accidents [1–3]. Depending on the fracture type and severity, different healing methods are used [4]. For high energy fractures involving significant bone debris, indirect healing (i.e., plastering) is often adopted. For simpler (low energy) fractures of long bones, direct healing, involving the direct application of internal fixation devices to the broken bones, is usually preferred. The healing of bone fractures may be primary or secondary [5]. Primary healing requires the precise anatomical realignment of fractured extremities without gaps, supporting direct and stable contact. For unstable and indirect contact, fractured bones heal by secondary healing, combining intramembranous and endochondral ossification [5]. Mechanical stimuli, such as stress and deformation, play a crucial role in secondary healing. Indeed, mechanical stress applied to fractured bone stimulates bone cells to produce new bone tissue, promoting bone callus formation and accelerating the healing process [6–8]. In addition, applying controlled stress levels to bone during remodeling contributes to increased bone density and the formation of more resistant bone tissue. Without sufficient surrounding stress, bone becomes fragile and unstable and may prematurely re-fracture after removal of the bone plate [8].

Bone plates are an important type of internal fixation device for stabilizing human bone fractures and are typically made of stainless steel and titanium alloys. Although metals have high strength, ductility, and wear resistance, they may undergo corrosion in physiological conditions, increased thermal conductivity, as well as be sensitive to electromagnetic fields [9–12]. Ti-6Al-4V has a Young's modulus five times higher than human cortical bone [13]. The significantly higher stiffness of metallic plates for bone fixation

with respect to cortical bones leads to the increased transfer of higher loads through plates rather than through bones. This phenomenon, referred to as the "stress shielding effect" or "stress protection", retards the natural bone healing process [14]. However, the presence of these metal plates in the human body for a long period of time may cause pain, infection, tissue irritation, etc. Therefore, they must be removed from the body after a certain period of time through secondary surgery. Other metal alloys, such as magnesium alloys, can naturally degrade in the human body. For example, the ZM21 alloy easily decomposes over time, thus eliminating the need for plate removal via secondary surgery. In the presence of chloride and at neutral pH, as in bodily fluids, Mg hydroxide can be transformed into the completely soluble Mg chloride (Equation (1)):

$$Mg(OH)_{2(s)} + 2HCL \rightarrow MgCl_{2(aq)} + 2H_2O \quad (1)$$

Magnesium is an essential element for the human body, acting as co-factor for many enzymes. However, a high concentration of magnesium (>1.05 mmol/L) in bodily fluid may not be tolerated. Witte et al. [15] and Yamasaki et al. [16] have shown that magnesium plays a key role in bone remodeling. In addition, the mechanical properties of magnesium are closer to that of natural bone than other metal alloys and biodegradable polymers, which may reduce the stress shielding effect commonly associated with metallic materials. The main problem with using magnesium biodegradable implants is that degradation rate of pure Mg in physiological conditions is very high. Such a high degradation rate may cause the structural integrity of Mg implants to vanish before completing the bone healing process. Recently, several magnesium alloys have been investigated for use in biodegradable implants [17–19]. The AZ series alloys (aluminum and zinc) are the most investigated, mainly because of their commercial availability, showing less degradation than pure magnesium. The addition of calcium to magnesium alloys has improved degradation behavior. In addition, various coating technologies, such as polymeric, ceramic, and even metallic coating, have been developed for magnesium alloys in order to reduce initial degradation [20]. Degradation tests have shown, for example, that hydroxyapatite particles stabilize the degradation rate and present more uniform degradation in artificial seawater and cell solutions [21].

Another way to minimize stress shielding is to change the geometry of the bone fixation plate. The equivalent stiffness of metal parts and the material consumption in manufacturing processes may be adjusted by integrating topology optimization and additive manufacturing [22]. An alternative solution to stress shielding is to find innovative materials for fixation plates: the basic requirement is that the elastic modulus of fixation materials should be as close as possible to the bone modulus [22]. In the last decade, composite materials have had a significant impact in the field of prosthetic implants, with a particular focus on bone fixation plates [23–25]. Recent studies [26,27] have been actively exploring the use of composites in bone fixation plates due to their ability to improve properties such as strength, stiffness, and corrosion resistance. In clinical applications, carbon fiber reinforced PEEK (CF/PEEK) plates are radiolucent and do not obstruct radiographic analysis; hence, their CT images have much less artifacts than those recorded for metal alloy fixation plates [28]. In addition, as shown above, metal ions released from metal implants can cause allergic reactions in tissues, as the body may react with hypersensitivity to such materials. Replacing metal with CF/PEEK can prevent this potential hypersensitivity, because this composite does not release metal ions, thus reducing the risk of allergic reactions in surrounding tissues [29].

For the purpose of developing high-performance composite bone plates with mechanical properties that promote bone fracture healing, several research studies have been conducted. Fujihara et al. [30] investigated the manufacturing process of carbon/PEEK thermoplastic bone plates; mechanical performance was partially verified by comparing experimental data gathered from 4-point bending tests with analytical results. Kim et al. [31] compared the mechanical performance of a composite bone plate with a commercially available stainless steel bone plate then determined the best conditions for the composite plate.

In evaluating the best performance of composite bone plates, the callus stress distributions generated between the fracture surfaces were considered an important criterion. Following this rationale, the present study utilized the finite element method (FEM) to analyze and evaluate the effect of stress shielding, in terms of stress transmission to bone, on a tibial fracture fixed by a titanium alloy plate, a magnesium alloy plate, and a composite material (carbon fiber reinforced PEEK, CFRP) plate.

The manuscript is organized as follows: Section 2 describes the geometric modeling and the finite element modeling/analysis of the fixation plate. Section 3 presents the results of FE simulations relative to the different materials of the fixation plates. Section 4 discusses the results while in view of the limitations of the study. Section 5 summarizes the main findings of the study and outlines future research directions.

2. Materials and Methods

2.1. Model Geometry

This study focuses on the fixation of tibial fractures with composite material plates. The tibia, one of the main load-bearing bones of the human leg, is shown in Figure 1. It transfers loads between the foot and femur during standing or walking. Similar to other bones, the outer part of bone is made up of cortical bone, while the core is made up of trabecular bone. Cortical bone is composed of hard, dense tissue and is involved in load transfer, such as flexion and compression. In contrast, the trabecular part is composed of spongy tissue to reduce structural mass [31,32].

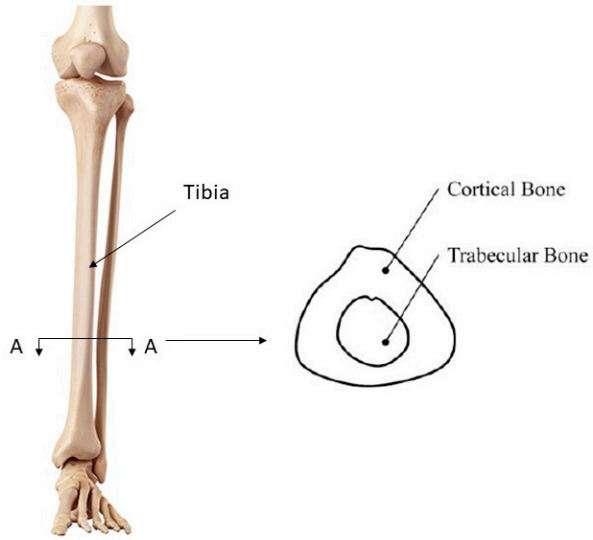

Figure 1. 3D view of the tibia bone and details of the bone cross-section highlighting the cortical and trabecular regions.

To simplify the geometry, the tibia was modeled as a hollow cylinder. The geometric specifications of the tibia (averaged from anatomical databases) were 10 mm inner diameter, 25 mm outer diameter, 103 mm total length (see Figure 2) [32]. This model was used to perform finite element simulations for evaluating the structural behavior of the tibia and the fixation devices used during the healing process.

The fracture site was assumed to have 1 mm thickness [32], with the outer and inner diameters corresponding to those of the tibia. The plate was modeled with six holes that crossed both the plate itself and the thickness of the bone. The plate dimensions were defined as length 68 mm, width 10 mm and thickness 3 mm. All three-dimensional models were created using Autodesk Inventor 2024 software.

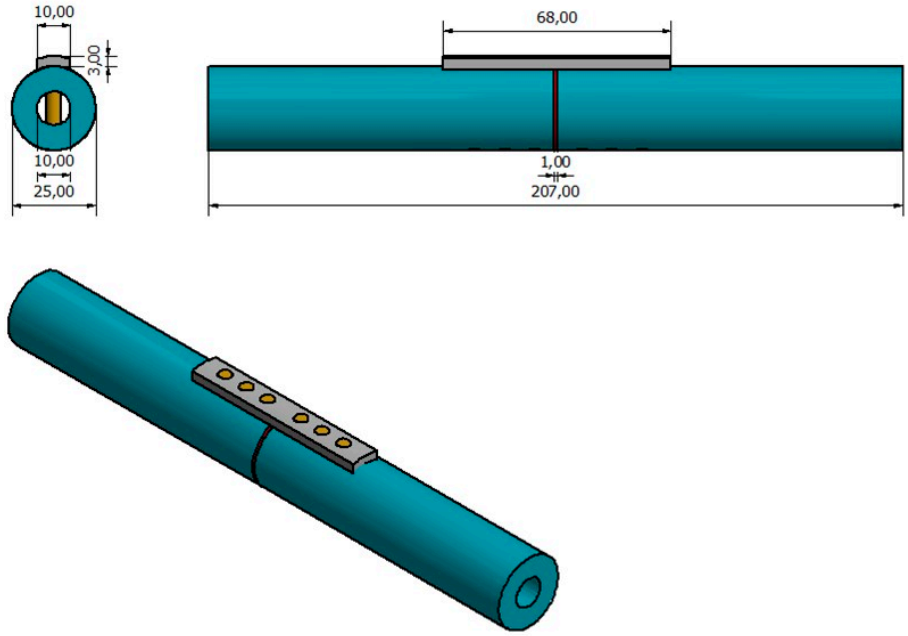

Figure 2. Detail of geometric dimensions assumed in 3D modeling of fractured bone and bone plate.

2.2. Material Properties

Bones are typically composed of cortical bone in the outer region and trabecular bone in the inner region [32], which have an anisotropic behavior. An anisotropic material is described by 21 elastic constants, but bone has been shown to exhibit transverse isotropic behavior in the YZ and XZ planes. Therefore, it can be described as an orthotropic model with 9 elastic constants (E_x, E_y, E_z, G_{xy}, G_{yz}, G_{xz}, ν_{xy}, ν_{yz}, ν_{xz}). Two stages of healing in the fractured debris (1% and 75%) were considered for analysis. It was assumed that the callus acts as a bridge at the fracture site, and that the callus material is homogeneous and isotropic [32]. Regarding bone plate materials, the following fixation plate materials were considered in this study.

- Titanium alloy, Ti-6Al-4V;
- Magnesium alloy, ZM21;
- Carbon fiber reinforced PEEK (CFRP) composite material.

On the other hand, CFRP mechanical behavior depends on the fibers' mechanical properties as well as on the fibers' orientation in the different layers. In this study, configuration I was selected, with fibers oriented at 0°, +45°, −45°, and 90°, where the 0° orientation corresponds to the longitudinal direction of the tibia. This configuration allows the optimal distribution of the applied load and results in a homogeneous mechanical behavior of the system [33–37]. The selected orientations of fibers help optimally distribute and transmit the applied load to the bone. In addition, mechanical behavior is transversely isotropic in this configuration. An approximately 60% fiber volume fraction was selected, as this is the critical volume below which mechanical properties of composite material are inferior to those of the matrix [38]. The mechanical properties of all materials used in the FEA of fixed bone are listed in Table 1 [38].

Table 1. Mechanical properties of all materials used in the FEA of fixed bone [32–38].

Material	E_x (GPa)	E_y (GPa)	E_z (GPa)	G_{xy} (GPa)	G_{yz} GPa)	G_{xz} (GPa)	v_{xy}	v_{yz}	v_{xz}
Bone	18.400	7.000	8.500	2.410	3.560	3.560	0.12	0.37	0.14
Fractured Bone	0.2 (1% healing) 15.00 (75% healing)						0.3 0.3		

Table 1. *Cont.*

Material	E_x (GPa)	E_y (GPa)	E_z (GPa)	G_{xy} (GPa)	G_{yz} GPa)	G_{xz} (GPa)	v_{xy}	v_{yz}	v_{xz}
Ti-6Al-4V	110	110	110				0.3		
Mg Alloy ZM 21	45	45	45				0.35		
CFRP	4	9.8	9.8	3.5	3	3.5	0.3	0.3	0.3

2.3. Loading and Kinematic Boundary Conditions

The osteogenic ability of bone is influenced by the level of principal stress generated by applied loading modes. Stress varies if the bone is subjected to compression, flexion, and torsion. It has been observed that the maximum principal stress under compression and flexion can favor osteogenesis more than torsion [32,38–41]. Therefore, the bone and fixation plate assembly were modeled here subject to compression and flexion, excluding the torsion case, as shown in Figure 3.

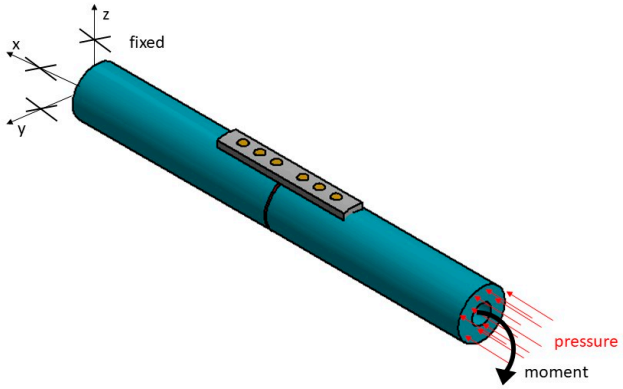

Figure 3. Loading and kinematic constraint conditions: The bone's left extremity was fixed, while a pressure of 1.1 MPa and a bending moment of 1 Nmm was applied on the bone's right extremity.

For a 90 kg patient standing on both legs, the magnitude of the load acting on the tibia cross-sectional area is approximately (Equation (2))

$$p = \frac{F}{A} = \frac{90 \times 10}{2 \times \pi\left[(12.5)^2 - 5^2\right]} = 1.1\ \text{MPa} \quad (2)$$

where p is the average pressure in the cross-sectional area of the bone (MPa), F is the body weight of the patient (N), and A is the cross-sectional area of fractured bone (mm^2). A bending moment of 1 Nmm was applied to the right end of the tibia, as shown in Figure 3. The bending moment simulates the conditions that promote callus formation in the fractured area, which contributes to the fracture healing process. When the bone fixation plate is applied to fracture, the callus-filled gap between the fracture faces deforms under muscle tension and weight bearing, causing the bone-plate assembly to bend. Consequently, strain is not uniform along the callus radial direction (ζ), as shown in Figure 4. In addition, a stiffer fixation plate distributes less stress to the bone than a less rigid plate (see Figure 4).

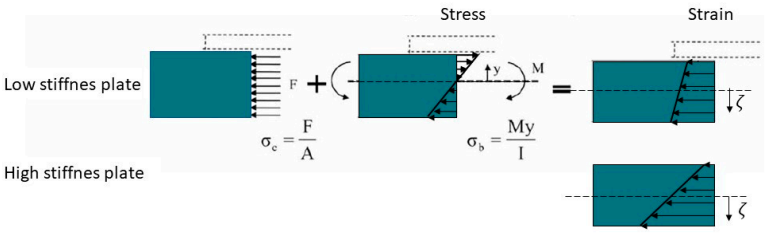

Figure 4. The effect of the bone plate modulus on callus and bone deformation.

2.4. Finite Element Model

The numerical simulation of the mechanical behavior of the plate-fractured bone assembly was performed with the commercial finite element code ANSYS Workbench© Version R2023. The geometric models were imported from Inventor 2024 and a mesh was then generated for all parts considered in the study. The SOLID 226 hexahedral element was selected for the static analysis [22,32,41,42]. To ensure the accuracy of results, convergence analysis was carried out to find the optimal mesh size. A coarser element size was initially selected and then gradually reduced until the average variation of nodal displacements between two successive iterations was less than 0.01%. The final mesh size was set to 1.5 mm for bone, fixation plate, and screws and 0.5 mm for the fractured bone area [32]. In total, the FE model included 336,257 nodes and 196,421 elements (see Figure 5).

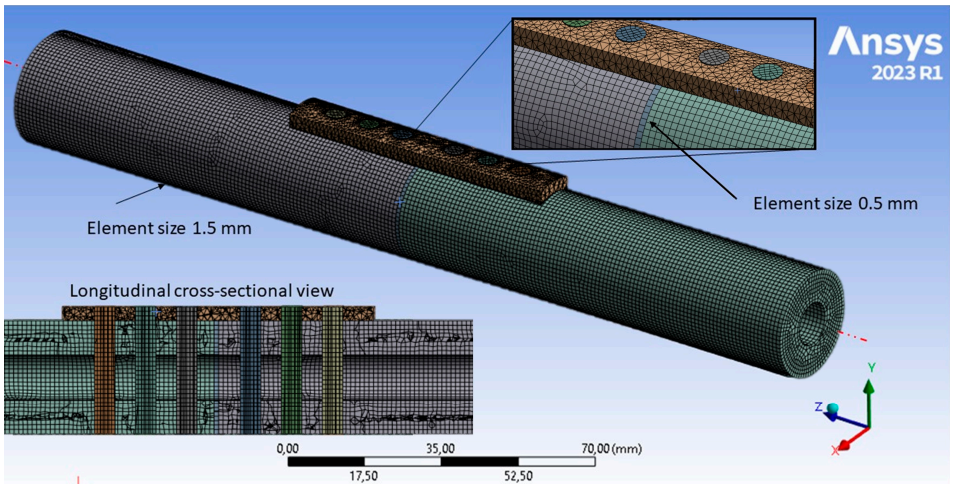

Figure 5. Mesh generation of the bone–bone fixation plate assembly.

To calculate behavior at the interfaces, two contact surfaces were defined between (i) the bone fixation plate and the tibial bone, (ii) screws and bone, and (iii) screws and bone fixation plate. A coefficient of friction of 0.4 was chosen between the plate and the bone [31]. Following Perren et al. [43], the appropriate traction force to stabilize fractures with the fixation plate in place ranges between 2000 and 3000 N. Higher screw fixation forces lead to excessive interface stress, causing blood flow problems in contact areas, while lower forces lead to excessive movement between bone plate and bone, resulting in ineffective bone stabilization. Therefore, a preload of 2000 N was applied to the screw. All screws were considered to be fixed in the bone.

3. Results

The von Mises equivalent stress distributions developed in the healing phases at 1% and 75% of the fractured area are shown in Figure 6, highlighting the influence of various bone fixation plate materials.

The von Mises stress gradually increases from the fixation plate side to the opposite side of bone. As expected, the minimum equivalent stress is localized on the fixation plate side that carries most of the load. In the beginning to 1% stage of fracture healing (approximately one week after surgery), there is no substantial hard tissue in the fracture gap. Therefore, the fracture site is characterized primarily by the presence of hematoma and fluid. These soft tissues are unable to withstand mechanical loads due to their relatively low Young's modulus. Consequently, stresses in the fractured area are relatively low for all bone plate materials, and the stress shielding caused by the fixation plate is at its highest level at the 1% healing stage compared to the 75% healing stage. Figure 6 shows how, at the 75% healing stage, more callus is formed: the callus becomes hard enough to support additional external loads. In fact, the stress distribution at this stage tends to be higher and more uniform in the bone. To analyze the stress distribution in the fractured area in detail,

three control points were defined, as shown in Figure 7. Specifically, point A is localized right below the fixation plate; point B is localized in the middle diameter of the bone; and point C is localized in the distal part of point A.

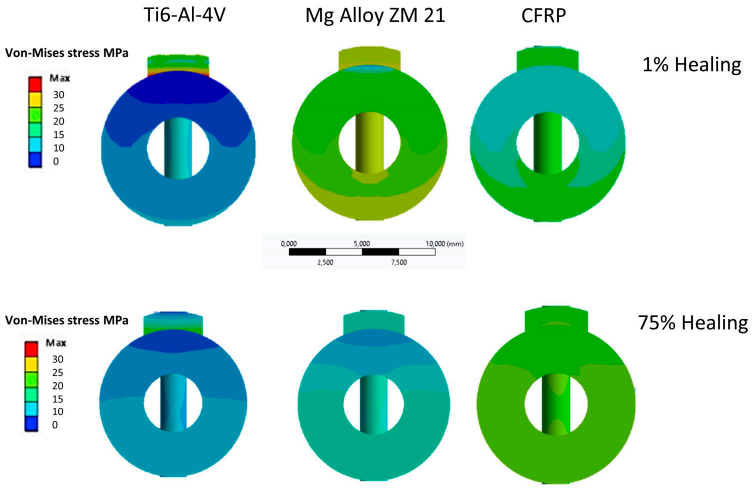

Figure 6. Distribution of Von Mises stress in fractured bone cross-sectional areas for different plate materials: 1% and 75% healing level.

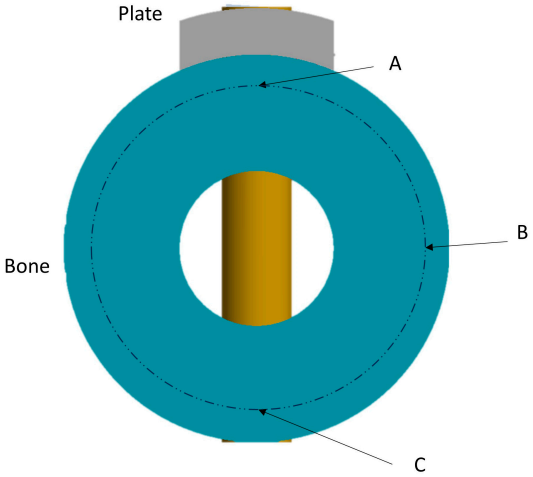

Figure 7. Positions of the three control points chosen for analyzing stress distribution in fractured bone.

Figure 8 shows the values of the von Mises stress at the control points A, B, and C, considering a healing phase of 1%.

For all fixation plates, the minimum stress occurs at point A, i.e., at the contact between the plate and the bone, with 1.12 MPa for the titanium alloy Ti-6Al-4V, 4.21 MPa for magnesium alloy ZM 21, and 7.35 MPa for the CFRP composite. It can also be observed that the stress increases as the control points move away from the plate. This can be explained because, looking at Figure 4, the stress changes linearly across the fractured bone section, with a point of minimum at the plate–bone contact, due to the phenomenon of stress shielding. In the 1% healing phase, the Ti-6Al-4V plate has a lower average stress in the bone than the other two plates. Since bone healing begins at the 1% healing stage, the generated tissues are not strong enough, and stress shielding is more evident.

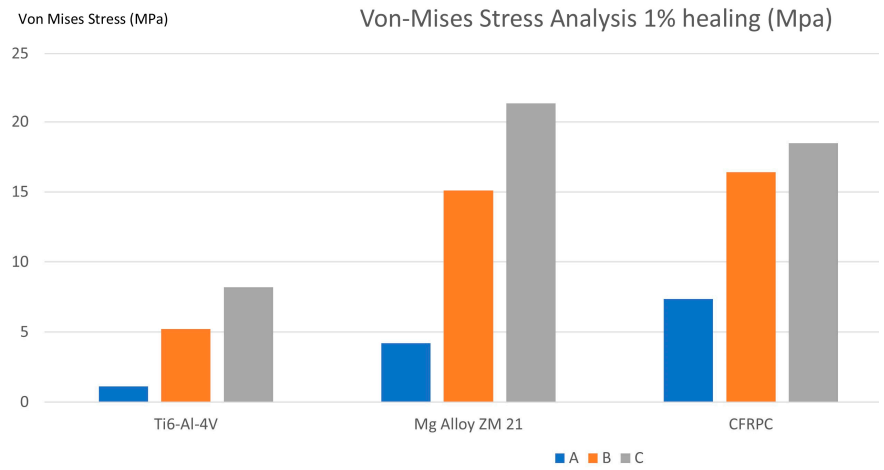

Figure 8. Von Mises stress values in fractured bone, considering different materials for the bone fixation plate and a healing stage of 1%.

Figure 9 shows the values of von Mises stress developed in the fractured bone at the 75% healing stage. Von Mises stress values at all control points of the fractured bone are higher than in the healing phase 1% for the titanium alloy and composite material. This can be explained with the argument that bone gains strength during healing due to external mechanical stimulation and can therefore absorb more stress and become more resistant. Using the CFRP fixation plate results in higher stresses in the bone than in the case of titanium and magnesium alloy plates (see Table 2).

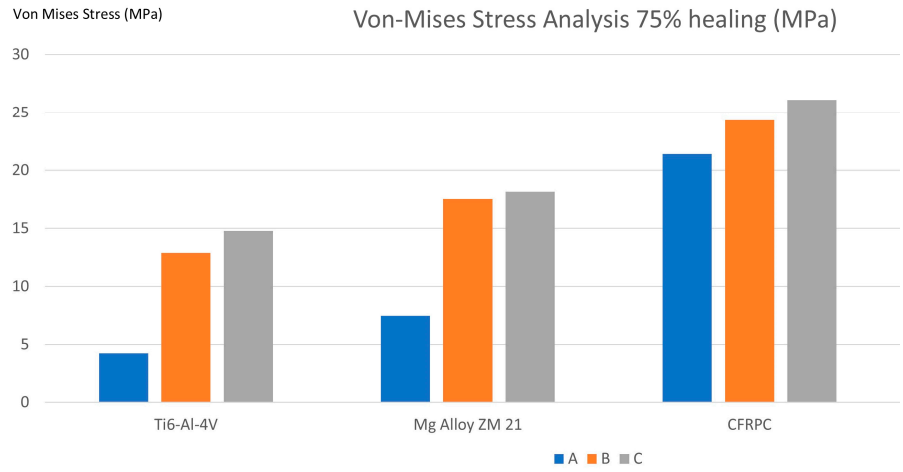

Figure 9. Von Mises stress values in fractured bone, considering different materials for the bone fixation plate and a healing stage of 75%.

Table 2. Von Mises stress values for different materials at the position (A, B, C) of the tibia, for a healing phase of 75%.

Plate Material	A	B	C
Ti-6Al-4V	4.24 MPa	12.89 MPa	14.77 MPa
Mg Alloy ZM 21	7.47 MPa	17.52 MPa	18.14 MPa
CFRP	21.41 MPa	24.32 MPa	26.12 MPa

Figure 6 also shows that the stress distribution in the bone is more uniform with the CFRP tread at 75% healing. Thus, the effect of stress shielding is less significant for CFRP than for titanium and magnesium alloys. This can be explained by the fact that the stiffness

of CFRP is closer to that of bone than that of the two metallic materials (see Table 1. From the point of view of mechanical behavior, stress analysis within the bone plate, which serves as a structural component to support the fractured area, is of considerable importance. In the 1% healing phase, the fractured area is weak and has the least capacity to support external loads. Most of the load is carried by the bone fixation plate, resulting in the highest stress within the plate at this stage. Figure 10 shows stress distributions in fixation plates in the 1% healing phase.

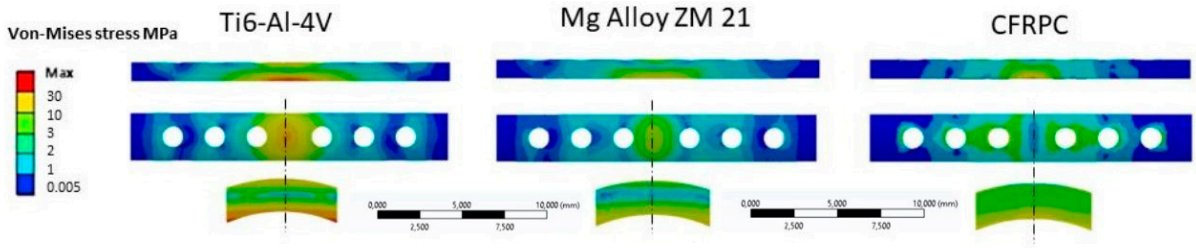

Figure 10. Von Mises stress distributions in the three bone fixation plates at the 1% healing stage.

It can be seen that stress concentration is highest in the two central screw holes near fracture site. This is because the fractured area is too weak to support external stress, and most stress is retained from the bone plate and screw, concentrating at the edge of the screw hole. From the cross-sectional view, it is possible to analyze the stress through the cross-section. Figure 10 shows that the most stressed plate is Ti-6Al-4V with 32 MPa of stress, followed by magnesium alloy ZM 21 with 25 MPa, and CFRP with 18.76 MPa. This shows that a stiffer material such as titanium absorbs most of the stress by shielding the bone from stress, therefore the stress shielding phenomenon is less evident when materials with mechanical properties closer to that of bone are used.

4. Discussion

Bone plates are the most used implants for the internal fixation of bone fractures. They present numerous advantages, including adequate stability and resistance to tension, compression, creep, torsion, and bending [44,45]. These are important characteristics for plates. They provide the support and strength necessary for proper fracture healing. In terms of materials, metal alloys such as 316 L stainless steel have been used in the manufacture of bone plates since 1895 [46]. However, due to high corrosion rates in human physiological environments and poor resistance to stress and wear, they were eliminated. Subsequently, titanium alloys such as Ti-6Al-4V were selected as candidates to replace steels. These alloys exhibit lower modulus, higher specific strength, superior biocompatibility, and improved corrosion resistance compared to stainless steels [47]. Resistance to corrosion from body fluids is provided by the presence of a passive TiO_2 film on the surface, which has the property of immediately reforming at body temperature and in physiological fluids, ensuring the excellent corrosion resistance of titanium alloy implants in vivo [48]. However, these materials present complex problems related to wear resistance and fatigue strength. These problems can lead to potential accidents such, as fractures and plate loosening [49].

The large difference in stiffness between metallic materials and bone causes stress shielding. This phenomenon occurs when a rigid orthopedic implant absorbs most of the load, preventing the surrounding bone tissue from performing its natural role of support and loading [50]. This can lead to problems such as reduced bone density and the risk of secondary fractures [51]. To overcome this problem, a material with similar strength and stiffness to bone must be chosen. Polymeric materials, such as PEEK, have been considered as an alternative to metallic materials for orthopedic implants [52]. Polymers are lightweight, easy to form, and can have a Young's modulus closer to that of bone tissue than metallic materials [52]. The inferior mechanical properties of polymeric fixation plates, compared to conventional titanium alloy plates, have been indicated as the main limitation of polymeric plates in several studies [52–55]. Particularly in skeletal sites

subject to loading, lower mechanical strength may have a negative impact on fracture stability. In fact, in a study by Schliemann et al. [56], the lower stiffness of the PEEK plate, together with the increased flexion and movement between bone and implant, contributed to increased movement in the fracture zone, resulting in a reduced load bearing capacity and, consequently, an earlier failure of fracture fixation.

Recently, magnesium (Mg) and its alloys proved to be promising biomaterials for bone plates due to their excellent mechanical properties, biocompatibility, and degradability in physiological fluids [57]. The Young's modulus of Mg is similar to that of cortical bone, which reduces stress shielding and promotes fracture healing [58]. Several studies have investigated Mg-based metallic materials for internal fracture fixation, with research focusing on reducing degradation rates and increasing corrosion resistance through methods such as CaP coating [59–62].

Looking at bone tissue, it is mainly composed of organic materials, such as collagen, and inorganic materials, such as hydroxyapatite. The organic materials are responsible for flexibility and strength, while the inorganic materials are responsible for hardness and compressive strength [63]. Composite materials inspired by this natural composition may achieve optimal mechanical properties [64–66]. In a study conducted by Sentihil Maharaj et al. [67], femoral bone fixation plates were developed using carbon fabric interwoven with flax fabric and bio-epoxy resin. Such a composite material was shown to have good strength and stiffness, like that of femur bone. This minimizes stress shielding. For example, the tensile strengths of stainless steel (515 MPa) and titanium (950 MPa) are much higher than that of femoral bone (139 MPa). A major advantage of polymer matrix composites is the possibility of tailoring mechanical performance based on several factors, including matrix type, reinforcement type, reinforcing phase particle size distribution, and reinforcing phase quantity. This flexibility allows composite properties to be tailored to the specific application [68].

Furthermore, Petersen et al. [69] found that carbon fiber-reinforced composites stimulate osseointegration more effectively than titanium, suggesting a potential improvement in biocompatibility and bone integration of implants. Furthermore, carbon fibers have conductive properties that may positively influence cellular activity. It is hypothesized that they may act as conductive micro-biocircuits, helping to remove damaging free radicals and improve the environment for cell growth.

The finite element method (FEM) can be used to study the stress distribution in bone tissues. The aim is to determine the possible causes of the stress shielding problem and how it can be reduced by modifying the material and geometry of the prosthetic element. For example, Ceddia et al. [22] carried out topology optimization of a femoral prosthesis made of CF/PEEK composite. Remarkably, the total mass of the prosthesis was reduced by 30% while maximum stress decreased from 987 MPa to about 810 MPa. However, the results shown in this study confirmed the theory that a material of similar stiffness to bone can equalize the stress distribution in bone by reducing the phenomenon of stress shielding. This explains why the magnesium alloy fixation plate reached its stress peak at the 1% healing phase. Conversely, the composite CFRP fixation showed more uniform and consistent stress distributions in the bone at the 1% and 75% healing stages. Such a behavior makes CFRP an excellent first choice material to use for bone fixating plates.

Since this study included limitations such as the simplified numerical and geometric modeling of the tibia and the use of a limited set of loading conditions, FE results should be compared with experimental data gathered from in vitro/vivo tests to validate the numerical model proposed here. In addition, the implementation of dynamic loads could help to better understand the fatigue life of the materials studied in this work, providing clinicians and designers of orthopedic prostheses with optimized selection in reference to the patient's characteristics.

5. Conclusions

The study used finite element simulations to analyze the influence of different types of materials: titanium alloy Ti-6Al-4V, magnesium alloy ZM21, and the composite material CFRP. Simulation results carried out on a simplified but realistic model showed that the CFRP bone fixation plate had a higher bone loading capacity than both metallic plates. This was evident not only from stress values at the fracture site near the plate but also from the average bone stress values throughout the fracture site, which were highest for the CFRP fixation. Therefore, in view of the required physical and chemical properties for fracture healing, this study indicates the CFRP fixation plate as the most suitable material for the fracture healing process. In fact, CFRP allows a better and more uniform stress distribution to be achieved in the fracture area. The stress shielding phenomenon is more pronounced in the post-operative phase, when the bone is in the 1% healing phase, compared to the metal bone fixation plates currently used in biomedical and healthcare applications.

Author Contributions: Conceptualization, M.C. and B.T.; methodology, M.C.; software, M.C.; validation, B.T. and G.S.; formal analysis, M.C., L.L. and B.T.; investigation, M.C.; resources, M.C. and B.T.; data curation, M.C.; writing—original draft preparation, M.C. and B.T.; writing—review and editing, M.C., B.T., L.L. and M.T.; visualization, B.T. and L.L.; supervision, G.S. and B.T.; project administration, G.S. and B.T. All authors have read and agreed to the published version of the manuscript.

Funding: This research received no external funding.

Institutional Review Board Statement: Not applicable.

Informed Consent Statement: Not applicable.

Data Availability Statement: All experimental data to support the findings of this study are available by contacting the corresponding author upon request.

Conflicts of Interest: The authors declare no conflicts of interest.

References

1. Gordon, J.E.; O'Donnell, J.C. Tibia fractures: What should be fixed? *J. Pediatr Orthop.* **2012**, *32* (Suppl. S1), S52–S61. [CrossRef]
2. Beale, B.; McCally, R. Minimally invasive fracture repair of the tibia and fibula. *Vet. Clin. N. Am. Small. Anim. Pract.* **2020**, *50*, 183–206. [CrossRef]
3. Prasad, M.; Yadav, S.; Sud, A.; Arora, N.C.; Kumar, N.; Singh, S. Assessment of the role of fibular fixation in distal-third tibia-fibula fractures and its significance in decreasing malrotation and malalignment. *Injury* **2013**, *44*, 1885–1891. [CrossRef]
4. Einhorn, T.A.; Gerstenfeld, L.C. Fracture healing: Mechanisms and interventions. *Nat. Rev. Rheumatol.* **2015**, *11*, 45–54. [CrossRef]
5. Claes, L.; Recknagel, S.; Ignatius, A. Fracture healing under healthy and inflammatory conditions. *Nat. Rev. Rheumatol.* **2012**, *8*, 133–143. [CrossRef]
6. Marsell, R.; Einhorn, T.A. The biology of fracture healing. *Injury* **2011**, *42*, 551–555. [CrossRef]
7. Li, J.; Qin, L.; Yang, K.; Ma, Z.; Wang, Y.; Cheng, L.; Zhao, D. Materials evolution of bone plates for internal fixation of bone fractures: A review. *J. Mater. Sci. Technol.* **2020**, *36*, 190–208. [CrossRef]
8. Palanisamy, P.; Alam, M.; Li, S.; Chow, S.K.H.; Zheng, Y.P. Low-intensity pulsed ultrasound stimulation for bone fractures healing: A review. *J. Ultrasound Med.* **2022**, *41*, 547–563. [CrossRef]
9. Dhason, R.; Roy, S.; Datta, S. Metal and composite bone plates for B1 periprosthetic femoral fracture in healthy and osteoporotic condition: A comparative biomechanical study. *Int. J. Artif. Organs.* **2022**, *45*, 704–714. [CrossRef]
10. Samiezadeh, S.; Tavakkoli Avval, P.; Fawaz, Z.; Bougherara, H. On optimization of a composite bone plate using the selective stress shielding approach. *J. Mech. Behav. Biomed. Mater.* **2015**, *42*, 138–153. [CrossRef]
11. Iwai, T.; Omura, S.; Aoki, N.; Tohnai, I. Use of self-tapping metal screws for temporary fixation of a resorbable plate system in maxillofacial surgery. *J. Craniofac. Surg.* **2015**, *26*, 891–892. [CrossRef]
12. Zdero, R.; Gide, K.; Brzozowski, P.; Schemitsch, E.H.; Bagheri, Z.S. Biomechanical design optimization of distal femur locked plates: A review. *Proc. Inst. Mech. Eng. H J. Eng. Med.* **2023**, *237*, 791–805. [CrossRef]
13. Al-Tamimi, A.A.; Fernandes, P.R.A.; Peach, C.; Cooper, G.; Diver, C.; Bartolo, P.J. Metallic bone fixation implants: A novel design approach for reducing the stress shielding phenomenon. *Virtual Phys. Prototyp.* **2017**, *12*, 141–151. [CrossRef]
14. Al-Tamimi, A.A.; Peach, C.; Fernandes, P.R.; Cseke, A.; Bartolo, P.J.D.S. Topology optimization to reduce the stress shielding effect for orthopedic applications. *Procedia CIRP* **2017**, *65*, 202–206. [CrossRef]
15. Witte, F.; Kaese, V.; Haferkamp, H.; Switzer, E.; Meyer-Lindenberg, A.; Wirth, C.J.; Windhagen, H. In vivo corrosion of four magnesium alloys and the associated bone response. *Biomaterials* **2005**, *26*, 3557–3563. [CrossRef]

16. Yamasaki, Y.; Yoshida, Y.; Okazaki, M.; Shimazu, A.; Kubo, T.; Akagawa, Y.; Uchida, T. Action of FGMgCO 3Ap–collagen composite in promoting bone formation. *Biomaterials* **2003**, *24*, 4913–4920. [CrossRef]
17. Castellani, C.; Lindtner, R.A.; Hausbrandt, P.; Tschegg, E.K.; Stanzl-Tschegg, S.; Zanoni, G.; Beck, S.; Weinberg, A.M. Bone-implant interface strength and osseointegration: Biodegradable magnesium alloy versus standard titanium control. *Acta Biomater.* **2011**, *7*, 432–440. [CrossRef] [PubMed]
18. Du, Z.; Yu, X.; Nie, B.; Zhu, Z.; Ibrahim, M.; Yang, K.; Tan, L.; Wang, Y. Effects of magnesium coating on bone-implant interfaces with and without polyether-ether-ketone particle interference: A rabbit model based on porous Ti6Al4V implants. *J. Biomed. Mater. Res. B Appl. Biomater.* **2019**, *107*, 2388–2396. [CrossRef]
19. Nasr Azadani, M.; Zahedi, A.; Bowoto, O.K.; Oladapo, B.I. A review of current challenges and prospects of magnesium and its alloy for bone implant applications. *Prog. Biomater.* **2022**, *11*, 1–26. [CrossRef]
20. Yang, Y.; Wu, Y.; Wei, Y.; Zeng, T.; Cao, B.; Liang, J. Preparation and characterization of hydroxyapatite coating on AZ31 magnesium alloy induced by carboxymethyl cellulose dopamine. *Materials* **2021**, *14*, 1849. [CrossRef]
21. Gu, X.; Zhou, W.; Zheng, Y.; Cheng, Y.; Wei, S.; Zhong, S.; Xi, T.F.; Chen, L.J. Corrosion fatigue behaviors of two biomedical Mg alloys—AZ91D and WE43 in simulated body fluid. *Acta Biomater.* **2010**, *6*, 4605–4613. [CrossRef]
22. Ceddia, M.; Trentadue, B.; De Giosa, G.; Solarino, G. Topology optimization of a femoral stem in titanium and carbon to reduce stress shielding with the FEM method. *J. Compos. Sci.* **2023**, *7*, 298. [CrossRef]
23. Wang, J.; Dou, J.; Wang, Z.; Hu, C.; Yu, H.; Chen, C. Research progress of biodegradable magnesium-based biomedical materials: A review. *J. Alloys Compd.* **2022**, *923*, 166377. [CrossRef]
24. Ortega-Martínez, J.; Farré-Lladós, M.; Cano-Batalla, J.; Cabratosa-Termes, J. Polyetheretherketone (PEEK) as a medical and dental material. A literature review. *Med. Res. Arch.* **2017**, *5*, 1–16. [CrossRef]
25. Mehboob, H.; Chang, S.-H. Effect of structural stiffness of composite bone plate–scaffold assembly on tibial fracture with large fracture gap. *Compos. Struct.* **2015**, *124*, 327–336. [CrossRef]
26. Liao, C.; Li, Y.; Tjong, S.C. Polyetheretherketone and its composites for bone replacement and regeneration. *Polymers* **2020**, *12*, 2858. [CrossRef]
27. Hassani, K.; Nikkhoo, M.; Karimi, A. The role of the fiber ply configurations on the biomechanics of the hip prosthesis. *Int. J. Model. Simul. Sci. Comp.* **2022**, *13*, 2250017. [CrossRef]
28. Abdellah, M.Y.; Alharthi, H.; Hassan, M.K.; Mohamed, A.F. Effect of specimen size on natural vibration of open hole copper/glass-reinforced epoxy laminate composites. *AIMS Mater. Sci.* **2020**, *7*, 499–517. [CrossRef]
29. Laux, C.J.; Hodel, S.M.; Farshad, M.; Müller, D.A. Carbon fibre/polyether ether ketone (CF/PEEK) implants in orthopaedic oncology. *World J. Surg. Oncol.* **2018**, *16*, 241. [CrossRef]
30. Fujihara, K.; Huang, Z.M.; Ramakrishna, S.; Satknanantham, K.; Hamada, H. Feasibility of knitted carbon/PEEK composites for orthopedic bone plates. *Biomaterials* **2004**, *25*, 3877–3885. [CrossRef]
31. Kim, S.H.; Chang, S.H.; Jung, H.J. The finite element analysis of a fractured tibia applied by composite bone plates considering contact conditions and time-varying properties of curing tissues. *Compos. Struct.* **2010**, *92*, 2109–2118. [CrossRef]
32. Zhang, C.; Wen, P.; Xu, Y.; Fu, Z.; Ren, G. Exploring advanced functionalities of carbon fiber-graded PEEK composites as bone fixation plates using finite element analysis. *Materials* **2024**, *17*, 414. [CrossRef]
33. Fouda, N.; Mostafa, R.; Saker, A. Numerical study of stress shielding reduction at fractured bone using metallic and composite bone-plate models. *Ain Shams Eng. J.* **2019**, *10*, 481–488. [CrossRef]
34. Benli, S.; Aksoy, S.; Havıtcıoglu, H.; Kucuk, M. Evaluation of bone plate with low-stiffness material in terms of stress distribution. *J. Biomech.* **2008**, *41*, 3229–3235. [CrossRef]
35. Shirurkar, A.; Tamboli, A.; Jagtap, P.N.; Dondapati, S.; Davidson, J.D. Mechanical behavior of ZM21 magnesium alloy locking plates–an experimental and finite element study. *Mater. Today Proc.* **2017**, *4*, 6728–6736. [CrossRef]
36. Guo, L.; Naghavi, S.A.; Wang, Z.; Varma, S.N.; Han, Z.; Yao, Z.; Wang, L.; Wang, L.; Liu, C. On the design evolution of hip implants: A review. *Mater. Des.* **2022**, *216*, 110552. [CrossRef]
37. Chang, L.; Wang, H.; Guo, Y.; Cai, Z.; Zhan, H. Experimental and numerical analysis of biomechanical effects in cervical spine positioning rotation manipulation. *Int. J. Numer. Methods Biomed. Eng.* **2022**, *38*, e3651. [CrossRef]
38. Ceddia, M.; Solarino, G.; Giannini, G.; De Giosa, G.; Tucci, M.; Trentadue, B. A Finite element analysis study of influence of femoral stem material in stress shielding in a model of uncemented total hip arthroplasty: Ti-6Al-4V versus carbon fibre-reinforced PEEK composite. *J. Compos. Sci.* **2024**, *8*, 254. [CrossRef]
39. Darwich, A.; Nazha, H.; Daoud, M. Effect of coating materials on the fatigue behavior of hip implants: A three-dimensional finite element analysis. *J. Appl. Comput. Mech.* **2020**, *6*, 284–295.
40. Ganesh, V.K.; Ramakrishna, K.; Ghista, D.N. Biomechanics of bone-fracture fixation by stiffness-graded plates in comparison with stainless-steel plates. *Biomed. Eng. Online* **2005**, *4*, 46. [CrossRef]
41. Lanyon, L.E. Using functional loading to influence bone mass and architecture: Objectives, mechanisms, and relationship with estrogen of the mechanically adaptive process in bone. *Bone* **1996**, *18*, S37–S43. [CrossRef]
42. Ahirwar, H.; Gupta, V.K.; Nanda, H.S. Finite element analysis of fixed bone plates over fractured femur model. *Comput. Methods Biomech. Biomed. Eng.* **2021**, *24*, 1742–1751. [CrossRef]
43. Perren, S.M. Evolution of the internal fixation of long bone fractures. The scientific basis of biological internal fixation: Choosing a new balance between stability and biology. *J. Bone Joint. Surg.* **2002**, *84*, 1093–1110. [CrossRef]

44. Pater, T.J.; Grindel, S.I.; Schmeling, G.J.; Wang, M. Stability of unicortical locked fixation versus bicortical non-locked fixation for forearm structures. *Bone Res.* **2014**, *2*, 14014. [CrossRef]
45. Nourisa, J.; Rouhi, G. Biomechanical evaluations of intramedullary nail and bone plate for the fixation of distal metaphyseal fractures. *J. Mech. Behav. Biomed. Mater.* **2016**, *56*, 34–44. [CrossRef]
46. Niinomi, N. Recent metallic materials for biomedical applications. *Metall. Mater. Trans. A* **2002**, *33*, 477–486. [CrossRef]
47. Al-Shalawi, F.D.; Mohamed Ariff, A.H.; Jung, D.W.; Mohd Ariffin, M.K.A.; Seng Kim, C.L.; Brabazon, D.; Al-Osaimi, M.O. Biomaterials as implants in the orthopedic field for regenerative medicine: Metal versus synthetic polymers. *Polymers* **2023**, *15*, 2601. [CrossRef]
48. Szewczenko, J.; Marciniak, J.; Kajzer, W.; Kajzer, A. Evaluation of corrosion resistance of titanium alloys used for medical implants. *Arch. Metall. Mater.* **2016**, *61*, 695–700. [CrossRef]
49. Azevedo, C.R.F. Failure analysis of a commercially pure titanium plate for osteosynthesis. *Eng. Fail. Anal.* **2003**, *10*, 153–164. [CrossRef]
50. Chandra, G.; Pandey, A. Design approaches and challenges for biodegradable bone implants: A review. *Expert Rev. Med. Devices* **2021**, *18*, 629–647. [CrossRef]
51. Kennady, M.C.; Tucker, M.R.; Lester, G.E.; Buckley, M.J. Stress shielding effect of rigid internal fixation plates on mandibular bone grafts. A photon absorption densitometry and quantitative computerized tomographic evaluation. *Int. J. Oral Maxillofac. Surg.* **1989**, *18*, 307–310. [CrossRef]
52. Kennedy, S.M.; Vasanthanathan, A.; Robert, R.B.J.; Amudhan, K. Advancements and prospects of polymer-based hybrid composites for bone plate applications. *Polym-Plast. Technol. Mater.* **2024**, *63*, 68–87. [CrossRef]
53. Chandra, G.; Pandey, A. Preparation strategies for Mg-alloys for biodegradable orthopaedic implants and other biomedical applications: A review. *Irbm* **2022**, *43*, 229–249. [CrossRef]
54. Abd Razak, S.I.; Ahmad Sharif, N.F.; Abdul Rahman, W.A.W. Biodegradable polymers and their bone applications: A review. *Int. J. Basic Appl. Sci.* **2012**, *12*, 31–49.
55. Cox, T.; Kohn, M.W.; Impelluso, T. Computerized analysis of resorbable polymer plates and screws for the rigid fixation of mandibular angle fractures. *Int. J. Oral Maxillofac. Surg.* **2003**, *61*, 481–487. [CrossRef]
56. Schliemann, B.; Wähnert, D.; Theisen, C.; Herbort, M.; Kösters, C.; Raschke, M.J.; Weimann, A. How to enhance the stability of locking plate fixation of proximal humerus fractures? An overview of current biomechanical and clinical data. *Injury* **2015**, *46*, 1207–1214. [CrossRef]
57. Byun, S.H.; Lim, H.K.; Cheon, K.H.; Lee, S.M.; Kim, H.E.; Lee, J.H. Biodegradable magnesium alloy (WE43) in bone—Fixation plate and screw. *J. Biomed. Mater. Res. B Appl. Biomater.* **2020**, *108*, 2505–2512. [CrossRef]
58. Fischer, H.; Schmidt-Bleek, O.; Orassi, V.; Wulsten, D.; Schmidt-Bleek, K.; Heiland, M.; Steffen, C.; Rendenbach, C. Biomechanical comparison of WE43-based magnesium vs. titanium miniplates in a mandible fracture model in sheep. *Materials* **2022**, *16*, 102. [CrossRef]
59. Zhi, P.; Liu, L.; Chang, J.; Liu, C.; Zhang, Q.; Zhou, J.; Liu, Z.; Fan, Y. Advances in the study of magnesium alloys and their use in bone implant material. *Metals* **2022**, *12*, 1500. [CrossRef]
60. He, M.; Chen, L.; Yin, M.; Xu, S.; Liang, Z. Review on magnesium and magnesium-based alloys as biomaterials for bone immobilization. *J. Mater. Res. Technol.* **2023**, *23*, 4396–4419. [CrossRef]
61. Antoniac, I.; Miculescu, M.; Mănescu, V.; Stere, A.; Quan, P.H.; Pältânea, G.; Robu, A.; Earar, K. Magnesium-based alloys used in orthopedic surgery. *Materials* **2022**, *15*, 1148. [CrossRef] [PubMed]
62. Luo, Y.; Wang, J.; Ong, M.T.Y.; Yung, P.S.H.; Wang, J.; Qin, L. Update on the research and development of magnesium-based biodegradable implants and their clinical translation in orthopaedics. *Biomater. Transl.* **2021**, *2*, 188–196. [PubMed]
63. Perić Kačarević, Ž.; Rider, P.; Alkildani, S.; Retnasingh, S.; Pejakić, M.; Schnettler, R.; Gosau, M.; Smeets, R.; Jung, O.; Barbeck, M. An introduction to bone tissue engineering. *Int. J. Artif. Organs* **2020**, *43*, 69–86. [CrossRef]
64. Hsissou, R.; Seghiri, R.; Benzekri, Z.; Hilali, M.; Rafik, M.; Elharfi, A. Polymer composite materials: A comprehensive review. *Compos. Struct.* **2021**, *262*, 113640. [CrossRef]
65. Gupta, R.; Mitchell, D.; Blanche, J.; Harper, S.; Tang, W.; Pancholi, K.; Baines, L.; Bucknall, D.G.; Flynn, D. A review of sensing technologies for non-destructive evaluation of structural composite materials. *J. Compos. Sci.* **2021**, *5*, 319. [CrossRef]
66. Ceddia, M.; Trentadue, B. A review of carbon fiber-reinforced polymer composite used to solve stress shielding in total hip replacement. *AIMS Mater. Sci.* **2024**, *11*, 449–462. [CrossRef]
67. Senthil Maharaj, P.S.R.; Vasanthanathan, A. An insight into the mechanical and tribological behavior of carbon-flax reinforced bioepoxy hybrid composite bone plates for orthopedic applications. *Polym. Polym. Compos.* **2023**, *31*, 09673911231178444. [CrossRef]
68. Jafari Chashmi, M.; Fathi, A.; Shirzad, M.; Jafari-Talookolaei, R.A.; Bodaghi, M.; Rabiee, S.M. Design and analysis of porous functionally graded femoral prostheses with improved stress shielding. *Designs* **2020**, *4*, 12. [CrossRef]
69. Petersen, R. Carbon Fiber Biocompatibility for Implants. *Fibers* **2016**, *4*, 1. [CrossRef]